



# CHORUS

This is the accepted manuscript made available via CHORUS. The article has been published as:

## Structural transformations including melting and recrystallization during shock compression and release of germanium up to 45 GPa

P. Renganathan, Stefan J. Turneaure, Surinder M. Sharma, and Y. M. Gupta

Phys. Rev. B **99**, 134101 — Published 4 April 2019

DOI: [10.1103/PhysRevB.99.134101](https://doi.org/10.1103/PhysRevB.99.134101)

# **Structural Transformations Including Melting/Recrystallization during Shock Compression/Release of Germanium to 45 GPa**

P. Renganathan<sup>1</sup>, Stefan J. Turneaure<sup>1</sup>, Surinder. M. Sharma<sup>1</sup>, Y.M. Gupta<sup>1,2</sup>

<sup>1</sup>*Institute for Shock Physics, Washington State University, Pullman, Washington 99164, USA*

<sup>2</sup>*Department of Physics and Astronomy, Washington State University, Pullman, Washington 99164, USA*

## Abstract

Solid-solid and solid-liquid transformations were examined in Ge(100), using *in situ* x-ray diffraction measurements during uniaxial strain compression and release. For final stresses above 15.7 GPa, the Ge transformed to a highly textured tetragonal  $\beta$ -Sn phase. At 31.5 GPa and above, Ge transformed to the molten phase. Full stress release (uniaxial strain) from the  $\beta$ -Sn phase, from the melt boundary, and from the completely molten phase, resulted in reversion to an untextured cubic diamond (cd) phase. These findings demonstrate that the cd to  $\beta$ -Sn phase change is reversible, and that recrystallization from the liquid phase occurs on nanosecond timescales during release.

Shock compression is widely used to study various condensed state phenomena, including solid-solid transformations [1-6] and melting [7-10]. Plane shock wave experiments are well suited to examine structural transformations and their time-dependence, because the entire material can transform across a planar shock front on nanosecond time scales [1,2] and the loading conditions can be controlled precisely. Historically, structural transformations under shock compression have been studied primarily using continuum-scale measurements [1-10]. In the past two decades, experiments have utilized flash x-ray and laser-based x-ray methods to examine high-pressure structures of shock compressed KCl [11,12] and Fe [13,14] using x-ray diffraction (XRD) measurements. Single crystal studies are useful in providing insight into the orientation relationships and atomistic pathways that link initial and transformed structures [11-14]. However, these single-pulse XRD measurements lacked temporal evolution and utilized a broad spectrum of unwanted x-rays.

Recent experimental advances utilizing new XRD capabilities – the Dynamic Compression Sector (DCS) at the Advanced Photon Source (Argonne, IL) has linked a variety of planar shock compression drivers to a third-generation synchrotron light source – have provided new insights into a number of structural transformations [15-18]. Similarly, XRD measurements using an x-ray free electron laser have examined phase transformation in shorter duration shock wave experiments [19,20].

Using the DCS capabilities, single crystal silicon (Si) was studied [15] to determine the orientation relations between the initial and final structures under shock compression. A highly textured simple hexagonal (sh) high-pressure phase was observed directly under shock compression [15]. In a subsequent study on Si [18], shock melting was observed at ~30-32 GPa stress with reversion to a mixture of cubic diamond (cd) and  $\beta$ -Sn structure upon stress release.

However, during unloading the Si sample did not experience well-defined uniaxial strain conditions.

An important general question regarding phase diagrams under dynamic compression is the applicability of phase boundaries determined from static compression experiments to dynamic loading. Inherently, there are two significant differences regarding structural transformations under static compression and under shock compression (uniaxial strain): (1) the many orders of magnitude shorter time duration under shock compression and (2) the occurrence of inelastic deformation, due to stress deviators, preceding the phase change under shock compression. Addressing the role of these differences will require studies under well-controlled compression/release.

Germanium (Ge), being isostructural to Si, is an ideal material to examine the above issues. Structural transformations in Ge have been studied extensively under static compression [21-23] and the high-pressure properties show remarkable similarities to Si [21,24] undergoing the same sequence of phase changes with increasing pressure. However, because of the larger and more polarizable core containing  $3d$  electrons, Ge has larger pressure ranges between high-pressure polymorphs compared to Si [25,26]. Under static compression, Ge is known to undergo only one solid-solid phase transition (cd to  $\beta$ -Sn phase at 11 GPa) below 75 GPa [21]. The Hugoniot for Ge [6] indicate that a phase transformation begins around 12 GPa, preceded by inelastic deformation around  $\sim 6$  GPa. Additionally, a theoretically calculated Hugoniot for Ge suggests that shocked Ge transforms to the  $\beta$ -Sn structure before melting at  $\sim 50$  GPa with negligible mixed phase region [27].

Due to its relatively large atomic number and associated x-ray scattering, thin Ge samples can be examined using XRD measurements in plate impact experiments with thicknesses (tens of micrometers) comparable to those used in laser shock experiments to compare results for different shock durations. Recent preliminary XRD measurements in laser shocked Ge suggested a solid-solid transition precedes melting [28]; because the focus was to demonstrate simultaneous phase contrast imaging (PCI) and XRD measurements, neither the transition stresses nor the structure of high-pressure crystalline phase(s) were reported. In contrast, analysis of recovered Ge samples, laser shocked to  $\sim 33$  GPa, and classical molecular dynamics (MD) simulations have reported that Ge amorphized under shock compression [29]. However, these results require further examination because time-scales of MD simulations and recovery experiments differ by many orders of magnitude. Furthermore, recovered samples are subjected to complex loading/unloading conditions very different from the uniaxial strain conditions under planar loading/unloading. These studies indicate a need to examine structural changes and transformation kinetics in shocked Ge using *in situ* XRD measurements during uniaxial strain compression and release.

We report on real-time *in situ* XRD measurements during plane shock compression/release of Ge(100) to examine solid-solid and melting transitions during compression and potential transitions during stress release. Germanium is ideal for examining possible crystallization during release, because  $dP/dT < 0$  for the cd/liquid phase boundary [27,30,31].

The experimental configuration for our experiments is shown in Figure 1. Flat optically polished LiF(100) impactors, accelerated to velocities ( $U_{pr}$ ) from 1.8-3.9 km/s, impacted thin ( $\sim 20$ -100  $\mu\text{m}$ ) Ge(100) plates backed by LiF(100) windows. Upon impact, shock waves

propagate through the germanium sample before reverberation between the window and the impactor result in a constant well-defined final stress between 15.7 and 40.6 GPa. Because of small sample thicknesses, multi-wave structures (elastic and inelastic waves preceding phase transformation wave) were not resolved in the Ge/LiF interface velocity measured using a VISAR [32]. XRD frames were obtained while the sample was in the well-defined final state. The initial stress in the Ge samples (peak stress) was  $\sim 10\%$  higher than the final state stress due to the impedance mismatch between Ge and LiF; throughout the manuscript, we refer to the final stresses applicable to the XRD measurements and the corresponding peak stresses are listed in Table S1 [33].

A framing x-ray area detector was used to record four XRD frames during the impact event with 153.4 ns interframe spacing. Two detector configurations were used: 150 mm diameter field of view with the beam-center at the detector center and a 75 mm diameter field of view with the beam-center offset horizontally. In each experiment, one frame was obtained while the shocked Ge was in a constant final state. Additionally, for Expts. 08, 10 and 11, a single frame was obtained in the fully released uniaxial strain state. Experimental parameters are listed in supplementary Table S1 [33]. Measured two-dimensional diffraction patterns were converted to one-dimensional line profiles using FIT2D software [34,35].

Representative evolution of XRD patterns measured during shock compression and release are shown in Figure 2 (Expt. 08). Figure 2(a) shows the pattern from the ambient state; Laue spots were not observed in this case. However, upon rotating the gun/Ge crystal by several degrees or when using the larger area detector (see supplementary Figure S2 [33]), single crystal Laue spots were observed, providing a precise crystal orientation. In the two frames after impact (Figures 2b and 2c), new diffraction rings are observed. In the third frame after impact (Figure

2d), the release wave from the LiF free surface had propagated back through the Ge sample; and the resulting diffraction pattern consists of three new smooth rings showing that the Ge transformed from the high-pressure phase to an untextured crystalline phase, upon stress release under uniaxial strain.

Figure 3(a) shows the diffracted intensities vs  $2\theta$  scattering angle for final stresses ranging from 15.7 GPa to 40.6 GPa. For these diffraction peaks, the intensity was integrated around the entire diffraction ring after masking the LiF diffraction spots. Two separate peaks are observed (near  $2\theta \approx 13^\circ$  and  $2\theta \approx 18^\circ$ ), and both shift to higher  $2\theta$  with increasing stress. A shoulder can be observed along the left edge of the first peak, suggesting it to be a superposition of two peaks. The localized arcs in the diffraction images demonstrate that the high-pressure phase of Ge is highly textured. Analyzing each localized arc of the ring individually, by integrating over a small azimuthal angle range, allowed us to discriminate between the diffraction peaks which appear to be overlapping in profiles generated by integration over the full ring. Figure 3(b) shows the results, after integration over a limited azimuthal range of each localized arc, from four different Ge experiments (Expts. 04-07:  $\sim 22.4$  GPa final stress). The integration clearly shows that each of the two peaks observed when integrating around the entire ring (Fig. 3a) is actually a combination of two closely spaced diffraction peaks. The diffraction peaks shown in Figure 3(b) match the  $\{200\}$ ,  $\{101\}$ ,  $\{220\}$  and  $\{211\}$  peaks of the tetragonal  $\beta$ -Sn structure [33]. The corresponding  $\beta$ -Sn lattice parameters are listed in supplementary Table S1 [33].

Although only the cd to  $\beta$ -Sn phase change was observed under static compression of Ge below 75 GPa, another metallic phase (bct-5) has been predicted theoretically to possibly precede the  $\beta$ -Sn phase [36]. Diffraction simulations using the bct-5 structure do not match the

measured peaks ruling out bet-5 as the high-pressure structure of shocked Ge. These findings unambiguously establish that Ge shocked from 15.7-30.8 GPa transforms to the  $\beta$ -Sn structure, the phase observed under static loading conditions at comparable pressures [21]. Figure 4 compares the pressure dependence of lattice parameters under shock compression and under static compression [23]; within experimental scatter, the two sets of lattice parameters show a good match [23]. Thus, there is overall agreement between the solid-solid transformations observed under static compression [21] and shock compression. As discussed in the Supplementary Material, care needs to be exercised in comparing data from these two types of experiments because of temperature differences. Our results are also broadly consistent with the volume compression from continuum shock work on Ge [6].

At 30.8 GPa, the sharp peaks of the high-pressure phase are accompanied by a broad diffuse peak indicating a solid-liquid mixed phase. Beyond 31.5 GPa, the sharp  $\beta$ -Sn diffraction peaks vanish leaving one broad diffuse peak, indicating complete melting of shocked Ge. Our observation of shock melting at a much lower stress than the theoretical prediction ( $\sim 50$  GPa in Ref. 27) suggests a need for more accurate theoretical multiphase Ge equations of state.

Figures 1(c)-1(e) show the XRD frames in the final compressed state for Ge single crystals shocked to stresses of 22.3 GPa, 27.8 GPa and 30.8 GPa, respectively. At 22.3 GPa, the diffraction pattern primarily has localized spots implying a highly textured  $\beta$ -Sn phase. When shocked to 27.8 GPa, these spots extend over a larger azimuthal range indicating less texture and at 30.8 GPa on the solid/liquid phase boundary, we observe distinct smooth rings that are narrower than the ring representing a liquid phase. These observations demonstrate that as the stress approaches the shock melting stress, the high-pressure  $\beta$ -Sn structure texture weakens significantly.

Figure 3(c) shows the diffracted intensities vs  $2\theta$  obtained under uniaxial strain after full release from 26.3 GPa ( $\beta$ -Sn structure), 30.8 GPa ( $\beta$ -Sn structure/liquid mixed phase), and 32.8 GPa (fully melted state). The red dashed-dotted lines in Figure 3(c) represent XRD simulations assuming the ambient cubic diamond (cd) structure. The simulated cd (111), (220), and (311) peak locations match the observed ones, demonstrating that Ge transforms back to the ambient cd phase upon stress release. These results demonstrate that the cubic diamond to  $\beta$ -Sn phase change is reversible under shock-compression/release on nanosecond timescales. Our results also establish that under planar stress (uniaxial strain) release, recrystallization from the liquid state to the cubic diamond structure occurs on nanosecond timescales.

Interestingly, the transformation of Ge from the low-pressure cubic diamond phase to the metallic  $\beta$ -Sn phase under static pressures at room temperature is believed to be reconstructive [21], and unloading from the  $\beta$ -Sn phase results in the recovery of several other denser metastable phases rather than the equilibrium cd structure [21,37,38]. However, the  $\beta$ -Sn phase reverts to the cd phase upon unloading in static compression experiments at higher temperatures (423–623 K) [37,38]. In our experiments, upon rapid (nanosecond timescale) release from the  $\beta$ -Sn phase we observed transformation to the equilibrium cubic diamond structure with no evidence for other metastable phases.

The previous claim of shock-induced amorphization of Ge, based on an examination of recovered laser-shocked Ge samples [29], is contradicted by our results. The crystallization to the cd phase from the shocked state (lacking long range order) observed in our *in situ* measurements, upon uniaxial strain stress release, indicates that the shocked Ge was liquid rather than a metastable amorphous phase. Furthermore, amorphous phases are known to arise under static compression due to kinetic frustration of a transformation between equilibrium crystalline

structures [39]; for Ge, the shock stress at which loss of long range order is observed  $\sim 31.5$  GPa is far from the next equilibrium crystalline structure (Imma) observed at  $\sim 75$  GPa [21], ruling out kinetic frustration. Our results highlight the importance of *in situ* measurements while the material is in a uniaxial strain state.

Given that both Ge and Si undergo the same sequence of structural transformations under static compression [21], it is useful to compare present Ge results with previous XRD results on Si obtained at DCS [15,18]. Shocked Si single crystals transformed directly to the simple hexagonal structure for shock stresses from 26-32 GPa before melting [15,18];  $\beta$ -Sn and Imma phases were not observed for the shock stresses examined. These results are consistent with the Si phase diagram observed under static compression. Similar to shocked Ge, the high-pressure XRD patterns for shocked Si exhibited significant preferred orientation up to  $\sim 30$  GPa before losing texture prior to complete melting near  $\sim 33$  GPa. The high degree of texture observed in shocked single crystal Si from 26-30 GPa [15,18] indicates that the equilibrium melt boundary was not reached, contradicting a recent claim of equilibrium shock melting of Si over a surprisingly wide stress range, 14-27 GPa [40]. Whereas only the cd phase was observed upon release of shocked Ge, both cd and  $\beta$ -Sn phases were observed upon release of shocked Si. However, unlike the present work, the Si release state was likely probed during non-uniaxial strain conditions, warranting further investigations into the release of shocked Si. Overall, plate impact *in situ* XRD experiments on both Ge and Si single crystals are broadly consistent with their static compression phase diagrams [21].

In summary, the present experimental results have demonstrated that shocked Ge transforms from the ambient cubic diamond structure to the tetragonal  $\beta$ -Sn structure above 15.7 GPa and to the liquid state beyond 31.5 GPa. The observation of a significant decrease in the  $\beta$ -

Sn phase texture as the shock melting stress is approached suggests that texture loss in the high-pressure phase of shocked single crystals may serve as a general indication of the temperature being near the solid-liquid phase boundary. Upon uniaxial strain stress release, high-pressure germanium phases (both solid and liquid) revert to the ambient cubic diamond phase indicating a reversible phase transformation under shock compression and release. These well-characterized experiments are the first to study and observe reversibility and recrystallization in a thermodynamically uniform, fully released state under uniaxial strain. Overall, we conclude that, for the stresses examined, the present results are consistent with the equilibrium Ge phase diagram determined from static compression experiments [21]; results from experiments on isostructural Si [15,18] lead to similar conclusions. Further investigations on other materials are required to assess the generality of these conclusions.

Travis Volz, Paulo Rigg and the staff of Dynamic Compression Sector are thanked for assistance with plate impact experiments, preparation of the x-ray beam and the measured x-ray flux spectrum. Dr. J. M. Winey is thanked for useful discussions. This publication is also based upon work supported by the DOE NNSA under Award No. DE-NA0002007. This publication is also based upon work performed at the Dynamic Compression Sector, which is operated by Washington State University under the U.S. Department of Energy (DOE)/National Nuclear Security Administration award no. DE-NA0002442. This research used resources of the Advanced Photon Source, a DOE Office of Science User Facility operated for the DOE Office of Science by Argonne National Laboratory under contract no. DE-AC02-06CH11357.

## **References**

- [1] D. Bancroft, E. L. Peterson, and S. Minshall, *J. Appl. Phys.* **27**, 291 (1956).
- [2] G. E. Duvall and R. A. Graham, *Rev. Mod. Phys.* **49**, 523 (1977).
- [3] J. M. Brown and R. G. McQueen, *J. Geophys. Res. Solid Earth* **91**, 7485 (1986).
- [4] J. L. Mosenfelder, P. D. Asimow, D. J. Frost, D. C. Rubie, and T. J. Ahrens, *J. Geophys. Res. Solid Earth* **114**, B01203 (2009).
- [5] W. H. Gust and E. B. Royce, *J. Appl. Phys.* **42**, 1897 (1971).
- [6] W. H. Gust and E. B. Royce, *J. Appl. Phys.* **43**, 4437 (1972).
- [7] R. G. McQueen and S. P. Marsh, *J. Appl. Phys.* **31**, 1253 (1960).
- [8] S. B. Kormer, M. V. Sinitsyn, G. A. Kirillov, and V.D. Urlin, *Sov. Phys. JETP* **21**, 689 (1965).
- [9] Q. Williams, R. Jeanloz, J. Bass, B. Svendsen, and T. J. Ahrens, *Science* **236**, 181 (1987).
- [10] J. H. Nguyen and N. C. Holmes, *Nature (London)* **427**, 339 (2004).
- [11] T. d'Almeida and Y. M. Gupta, *Phys. Rev. Lett.* **85**, 330 (2000).
- [12] S. J. Turneaure, Y. M. Gupta, and P. Rigg, *J. Appl. Phys.* **105**, 013544 (2009).

- [13] D. H. Kalantar, J. F. Belak, G. W. Collins, J. D. Colvin, H. M. Davies, J. H. Eggert, T. C. Germann, J. Hawreliak, B. L. Holian, K. Kadau, P. S. Lomdahl, H. E. Lorenzana, M. A. Meyers, K. Rosolankova, M. S. Schneider, J. Sheppard, J. S. Stölken, and J. S. Wark., Phys. Rev. Lett. **95**, 075502 (2005).
- [14] J. Hawreliak, J. D. Colvin, J. H. Eggert, D. H. Kalantar, H. E. Lorenzana, J. S. Stölken, H. M. Davies, T. C. Germann, B. L. Holian, K. Kadau, P. S. Lomdahl, A. Higginbotham, K. Rosolankova, J. Sheppard, and J. S. Wark., Phys. Rev. B **74**, 184107 (2006).
- [15] S. J. Turneure, N. Sinclair, and Y. M. Gupta, Phys. Rev. Lett. **93**, 094107 (2016).
- [16] P. Kalita, P. Specht, S. Root, N. Sinclair, A. Schuman, M. White, A. L. Cornelius, J. Smith, and S. Sinogeikin., Phys. Rev. Lett. **119**, 255701 (2017).
- [17] S. J. Tracy, S. J. Turneure, and T. S. Duffy, Phys. Rev. Lett. **120**, 135702 (2018).
- [18] S. J. Turneure, S. M. Sharma, and Y. M. Gupta, Phys. Rev. Lett. **121** 135701 (2018).
- [19] M. G. Gorman, R. Briggs, E. E. McBride, A. Higginbotham, B. Arnold, J. H. Eggert, D. E. Fratanduono, E. Galtier, A. E. Lazicki, H. J. Lee, H. P. Liermann, B. Nagler, A. Rothkirch, R. F. Smith, D. C. Swift, G. W. Collins, J. S. Wark, and M. I. McMahon., Phys. Rev. Lett. **115** 095701 (2015).
- [20] A. E. Gleason, C. A. Bolme, H. J. Lee, B. Nagler, E. Galtier, R. G. Kraus, R. Sandberg, W. Yang, F. Langenhorst & W. L. Mao., Nat Commun. **8** 1 1481 (2017).
- [21] A. Mujica, A. Rubio, A. Munoz, and R. J. Needs, Rev. Mod. Phys. **75**, 863 (2003).
- [22] J. C. Jamieson, Science **139**, 762 (1963).

- [23] X. J. Chen, Chao Zhang, Yue Meng, Rui-Qin Zhang, Hai-Qing Lin, Viktor V. Struzhkin, and Ho-kwang Mao., Phys. Rev. Lett. **106**, 135502 (2011).
- [24] M. I. McMahon, R. J. Nelmes, N. G. Wright, and D. R. Allan, Phys. Rev. B **50**, 739 (1994).
- [25] S. P. Lewis and M. L. Cohen, Solid State Commun. **89**, 483 (1994).
- [26] K. J. Chang and M. L. Cohen, Phys. Rev. B **34**, 8581 (1986).
- [27] S. D. Crockett, G. De Lorenzi-Venneri, J. D. Kress, and S. P. Rudin., J. Phys.: Conf. Ser. **500** 032006 (2014).
- [28] F. Seiboth, L. B. Fletcher, D. McGonegle, S. Anzellini, L. E. Dresselhaus-Cooper, M. Frost<sup>1</sup>, E. Galtier<sup>1</sup>, S. Goede, M. Harmand, H. J. Lee, A. L. Levitan, K. Miyanishi<sup>8</sup>, B. Nagler<sup>1</sup>, I. Nam, N. Ozaki, M. Rödel, A. Schropp, C. Spindloe, P. Sun<sup>1</sup>, J. S. Wark<sup>3</sup>, J. Hastings, S. H. Glenzer, and E. E. McBride., Appl. Phys. Lett. **112**, 221907 (2018).
- [29] Shiteng Zhao, Bimal Kad, Christopher E. Wehrenberg, Bruce A. Remington, Eric N. Hahn, Karren L. More, and Marc A. Meyers, Proc. Natl. Acad. Sci. USA. **114**, 9791 (2017).
- [30] A. Jayaraman, W. Klement, Jr. and G. C. Kennedy, Phys. Rev. **130**, 540 (1963).
- [31] F. P. Bundy, J. Chem. Phys. **41**, 3809 (1964).
- [32] L. M. Barker and R. E. Hollenbach, J. Appl. Phys. **43**, 4669 (1972).
- [33] See Supplemental Material for additional experimental details and results, and methods used for analyzing the diffraction simulations and results.
- [34] A. P. Hammersley, FIT2D: An introduction and overview. ESRF Internal Report,

ESRF97HA02T (1997).

[35] A. P. Hammersley, S. O. Svensson, M. Hanfland, A. N. Fitch, D. Hausermann, High Pressure Res. **14**, 235 (1996).

[36] D. Selli, I. A. Baburin, R. Martončák and S. Leoni, Sci. Rep. **3**, 1466 (2013).

[37] V. V. Brazhkin et. al, Phys. Rev. B **51**, 7549 (1995).

[38] G.A. Voronin, C. Pantea, T.W. Zerda, J. Zhang, L. Wang, and Y. Zhao, J. Phys. Chem. Solids **64**, 2113 (2003).

[39] S. M. Sharma and S. K. Sikka, Prog. Mater. Sci. **40**, 1 (1996).

[40] E. E. McBride, E. Emma, A. Krygier, A. Ehnes, Eric Galtier, M. Harmand, Z. Konôpková, H. J. Lee, H. P. Liermann, Bob Nagler, A. Pelka, M. Rödel, A. Schropp, R. F. Smith, C. Spindloe, D. C. Swift, F. Tavella, S. Toleikis, T. Tschentscher, J. S. Wark, A. Higginbotham, Nature Physics **15**, 89–94 (2019).

## Figures

Figure 1: (a) Experimental configuration used for XRD and shock wave profile measurements under planar impact loading. Pulsed x-rays ( $\sim 23.5$  keV energy,  $\sim 100$  ps duration, 153.4 ns apart) passed through the LiF projectile, Ge sample, and the LiF window. Diffracted x-rays from individual pulses were recorded on a framing area detector. (b) Ge/LiF interface velocity history recorded using VISAR [32]. (c), (d), (e) Representative XRD results obtained for Ge(100) single crystals shocked to stresses of 22.3 GPa (Expt. 07), 27.8 GPa (Expt. 09) and 30.8 GPa (Expt. 10), respectively. The large, and bright diffraction spots are from either the LiF impactor or the LiF window.

Figure 2: Temporally-resolved XRD results for Ge(100) crystal shocked to 26.3 GPa (Expt. 08). (a) Ambient Ge single crystal diffraction result; bright spot is from the LiF window. (b) and (c) XRD data in the shocked state; times listed are relative to impact time. The diffraction patterns correspond to a textured  $\beta$ -Sn phase; inner ring is composed of the  $\{200\}$  and  $\{101\}$  peaks, and the outer ring is composed of  $\{220\}$  and  $\{211\}$  peaks. The broad inner ring labeled PC is from the polycarbonate projectile. (d) The XRD data corresponds to Ge in the released state and show cubic diamond Ge diffraction rings. Weak spots between the  $\{111\}$  and  $\{220\}$  cd rings

corresponding to the  $\beta$ -Sn structure are due to finite x-ray detector phosphor decay time (ghosting); these are known to be  $\beta$ -Sn ghost peaks (not corresponding to the released material) because they have the same scattering angles as the  $\beta$ -Sn peaks in the shocked state.

Figure 3: (a) One-dimensional diffraction peaks – azimuthally integrated around the entire diffraction rings – for shock-compressed Ge(100). Below  $\sim 30.8$  GPa, the diffraction patterns of the high-pressure phase consist of two distinct peaks; for stress of 31.5 GPa and above, the diffracted intensity from the high-pressure phase consists of one broad peak indicating a molten phase. The  $2\theta$  values corresponding to the ambient cd peaks for polycrystalline Ge are marked at the bottom for comparison and the broad hump near  $2\theta=7^\circ$  is from the polycarbonate projectiles. (b) Diffraction peaks obtained by integrating over small azimuthal ranges for each localized diffraction arc observed in experiments (04)-(07) with  $\sim 22.4$  GPa final stress. Four distinct peaks are indexed to the  $\beta$ -Sn structure. (c) Measured (solid lines) and simulated (red dashed-dotted lines) cd diffraction peaks after release from stresses of 26.3 GPa, 30.8 GPa and 32.8 GPa. Background was subtracted from line profiles in (b) and (c), but not from line profiles in (a).

Figure 4:  $\beta$ -Sn Ge lattice parameters from this work (blue symbols) and from static compression (red symbols) [23]. Uncertainty in final stress from shock experiments is smaller than the symbol size.

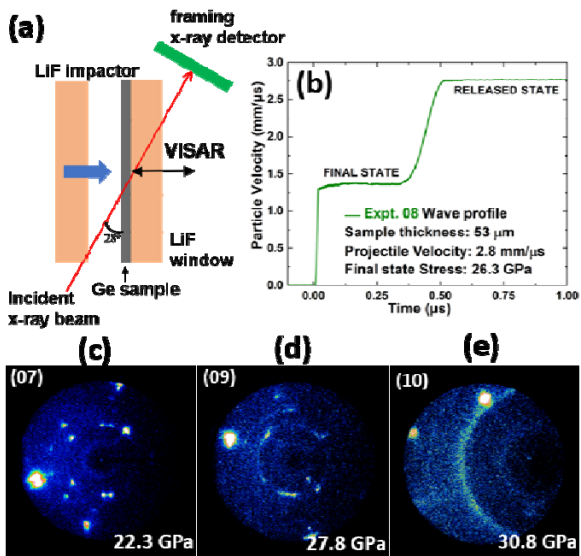


Figure 1

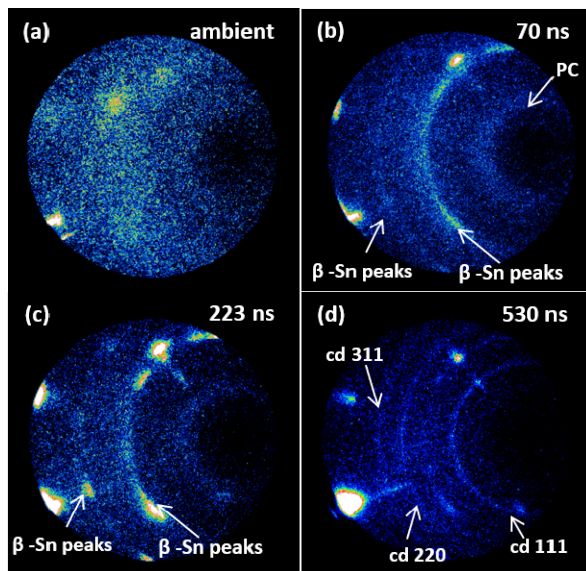


Figure 2

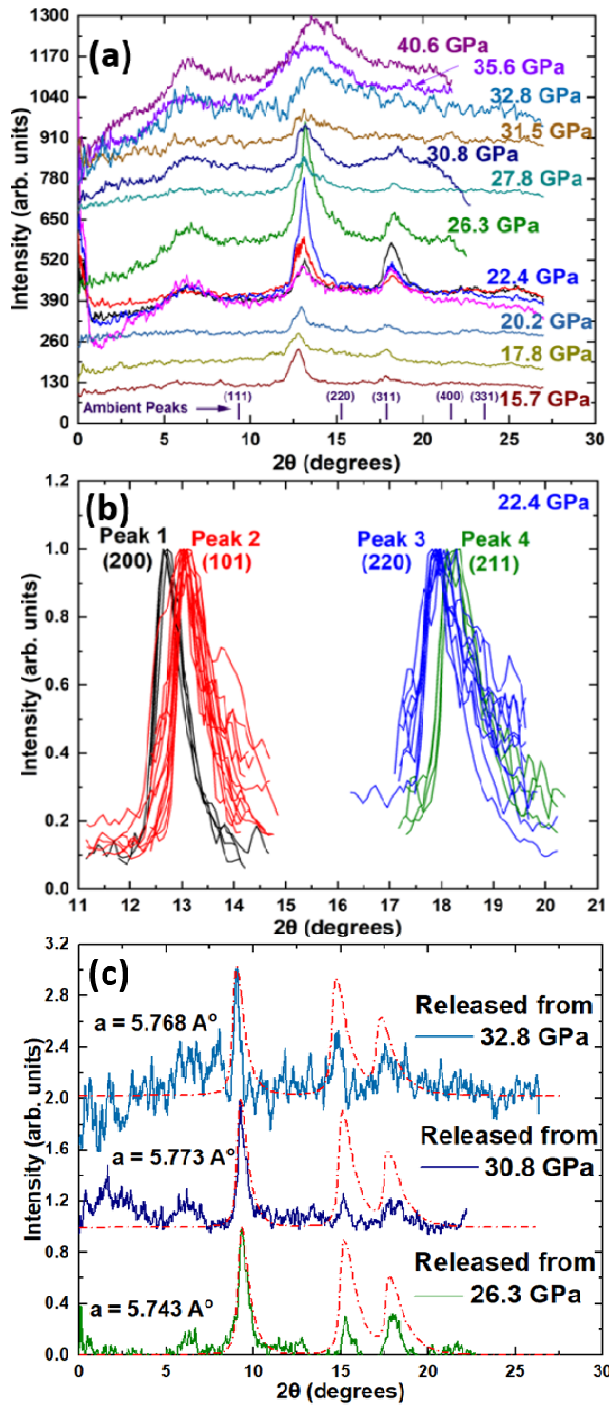


Figure 3

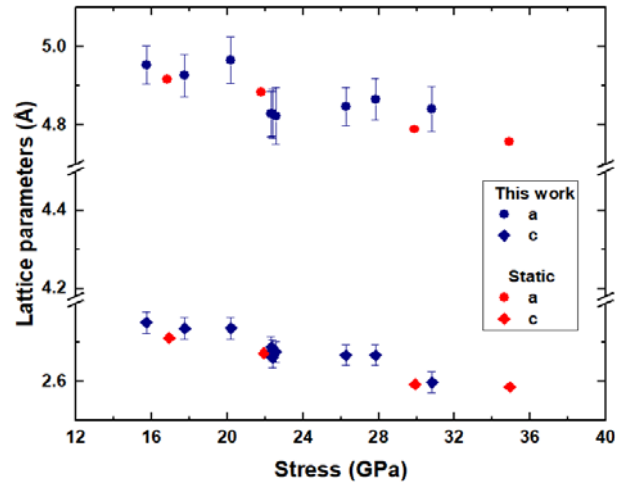


Figure 4